JACC: CARDIOVASCULAR IMAGING VOL. 6, NO. 3, 2013

ISSN 1936-878X/$36.00
PUBLISHED BY ELSEVIER INC. http://dx.doi.org/10.1016/j.jcmg.2012.06.016

Collagen-Specific Peptide Conjugated HDL Nanoparticles as MRI Contrast Agent to Evaluate Compositional Changes in Atherosclerotic Plaque Regression

Wei Chen, PhD,*† David P. Cormode, PhD,*† Yuliya Vengrenyuk, PhD,‡ Beatriz Herranz, PhD,*§ Jonathan E. Feig, MD, PhD,‡ Ahmed Klink, PhD,*‖ Willem J. M. Mulder, PhD,*¶ Edward A. Fisher, MD, PhD,‡ Zahi A. Fayad, PhD*†
New York, New York; Madrid, Spain; and Paris, France

OBJECTIVES This study sought to develop magnetic resonance contrast agents based on high-density lipoprotein (HDL) nanoparticles to noninvasively visualize intraplaque macrophages and collagen content in mouse atherosclerotic plaques.

BACKGROUND Macrophages and collagen are important intraplaque components that play central roles in plaque progression and/or regression. In a Reversa mouse model, plaque regression with compositional changes (from high macrophage, low collagen to low macrophage, high collagen) can be induced.

METHODS This study labeled HDL nanoparticles with amphiphilic gadolinium chelates to enable target-specific imaging of intraplaque macrophages. To render HDL nanoparticles specific for the extracellular matrix, labeled HDL nanoparticles were functionalized with collagen-specific EP3533 peptides (EP3533-HDL) via poly(ethylene glycol) spacers embedded in the HDL lipid layers. The association of nanoparticles with collagen was examined in vitro by optical methods. The in vivo magnetic resonance efficacy of these nanoparticles was evaluated in a Reversa mouse model of atherosclerosis regression. Ex vivo confocal microscopy was applied to corroborate the in vivo findings and to evaluate the fate of the different HDL nanoparticles.

RESULTS All nanoparticles had similar sizes (10 ± 2 nm) and longitudinal relaxivity r_1 (9 ± 1 s^{-1} $mmol/l^{-1}$). EP3533-HDL showed strong association with collagen in vitro. After 28 days of plaque regression in Reversa mice, EP3533-HDL showed significantly increased ($p < 0.05$) in vivo magnetic resonance signal in aortic vessel walls (normalized enhancement ratio [NER_w] = 85 ± 25%; change of contrast-to-noise ratio [ΔCNR_w] = 17 ± 5) compared with HDL ($NER_w = -7 \pm 23\%$; $\Delta CNR_w = -2 \pm 4$) and nonspecific control EP3612-HDL ($NER_w = 4 \pm 24\%$; $\Delta CNR_w = 1 \pm 6$) at 24 h after injection. Ex vivo confocal images revealed the colocalization of EP3533-HDL with collagen. Immunohistostaining analysis confirmed the changes of collagen and macrophage contents in the aortic vessel walls after regression.

CONCLUSIONS This study shows that the HDL nanoparticle platform can be modified to monitor in vivo plaque compositional changes in a regression environment, which will facilitate understanding plaque regression and the search for therapeutic interventions. (J Am Coll Cardiol Img 2013;6:373–84) © 2013 by the American College of Cardiology Foundation

From the *Translational and Molecular Imaging Institute, Icahn School of Medicine at Mount Sinai, New York, New York; †Department of Radiology, Translational and Molecular Imaging Institute, Icahn School of Medicine at Mount Sinai, New York, New York;

Atherosclerotic plaques are the result of a chronic inflammatory response in arterial vessel walls to the accumulated lipoproteins that contain apolipoprotein B (1). The rupture of a plaque may cause many severe health risks (2–4). Active inflammation with extensive macrophage infiltration into vessel walls, leading to plaques with a thin fibrous cap and a large lipid necrotic core are considered to be the major indicators, among several other factors, for high-risk plaques prone to rupture (5–11).

One of the therapeutic intervention goals for high-risk patients is to stabilize atherosclerotic lesions by inducing regression. In clinical studies, the stabilization of plaques has been found to correlate with lower intraplaque macrophages and higher interstitial collagen (12). Pre-clinical animal studies have further facilitated the understanding of plaque regression (12–15). Recently, the Fisher and Young groups developed the Reversa mouse model that possesses 4 homozygous alleles, $LDLR^{-/-}ApoB^{100/100}Mttp^{fl/fl}Mx1\text{-}Cre^{+/+}$ (16). When microsomal triglyceride transfer protein is conditionally ablated after plaque formation, low-density lipoprotein production falls, and the hyperlipidemic plasma profile abates, with a consequent regression of disease as indicated by a decrease of macrophages and increase of collagen in plaques (17). Although these changes in plaque component levels during regression have been confirmed by ex vivo histological examinations, noninvasive in vivo visualization methods to detect these biological events by molecular imaging are highly desired to allow temporal evaluation of the stabilization of atherosclerosis.

ABBREVIATIONS AND ACRONYMS

CNR = contrast-to-noise ratio

HDL = high-density lipoprotein

MR = magnetic resonance

NER = normalized enhancement ratio

PBS = phosphate-buffered saline

ROI = region of interest

SNR = signal-to-noise ratio

Magnetic resonance (MR) imaging is one of the most powerful techniques to noninvasively visualize plaque composition and biological activity at submillimeter spatial resolution (18,19). However, contrast agents with high payload are often essential for molecular MR imaging due to the low concentration of biomarkers and inherently low sensitivity of MR (20,21). We have previously developed high-density lipoprotein (HDL)-based MR contrast agents to evaluate intraplaque macrophage content via their natural affinity for plaque macrophages (22–26). In this study, we report the use of HDL-based MR contrast agents to visualize 2 key plaque components: macrophages and collagen during plaque regression conditions in Reversa mice. The HDL platform was used because of its endogenous nature, small size (~10 nm) that allows penetration into atherosclerotic plaques, and the possibility to include a higher contrast payload than small molecule platforms could. In addition, because plaque component changes in the duration of this study are more evident than size changes are (13,16,17), we were able to focus on changes in composition.

METHODS

Materials. The collagen-specific peptide EP-3533 with the sequence GKWH[CTTKFPHHYC] LYBip-$CONH_2$, and the nonspecific peptide EP-3612 containing non-natural *D*-Cys as shown in Figure 1 were synthesized by Peptide International (Louisville, Kentucky). 1,2-dimyristoyl-sn-glycero-3-phosphoethanolamine-*N*-(lissamine rhodamine B sulfonyl) (Avanti Polar Lipids, Inc., Alabaster, Alabama) and gadolinium diethylenetriaminepentaacetate-bis(stearylamide) (iQSynthesis, St. Louis, Missouri) were used as fluorescence label and MR contrast agents, respectively. The preparation of HDL nanoparticles followed our previous methods

‡Department of Medicine, Leon H. Charney Division of Cardiology and the Marc and Ruti Bell Program in Vascular Biology, New York University School of Medicine, New York, New York; §Department of Epidemiology, Atherothrombosis and Imaging, Fundacion Centro Nacional de Investigaciones Cardiovasculares Carlos III, Madrid, Spain; ‖Paris Cardiovascular Research Center, Institut National de la Santé et de la Recherche Médicale Assistance Publique-Hopitaux de Paris, Hopital Europeen Georges Pompidou, Paris, France; and the ¶Department of Gene and Cell Medicine, Icahn School of Medicine at Mount Sinai, New York, New York. This work was partially support by the following grants: NIH/NHLBI R01 HL71021, NIH/NBIB R01 EB009638, and NIH/NHLBI Program of Excellence in Nanotechnology (PEN) Award, HHSN268201000045C (to Dr. Fayad) and NHLBI P01HL098055, R01HL084312 (to Dr. Fisher). CSL Ltd. donated apolipoprotein A-I. Dr. Cormode has received research support from the National Institutes of Health, grant NIH K99 EB012165. All other authors have reported that they have no relationships relevant to the contents of this paper to disclose. Eike Nagel, MD, PhD, served as Guest Editor for this article.

Manuscript received February 7, 2012; revised manuscript received May 14, 2012, accepted June 29, 2012.

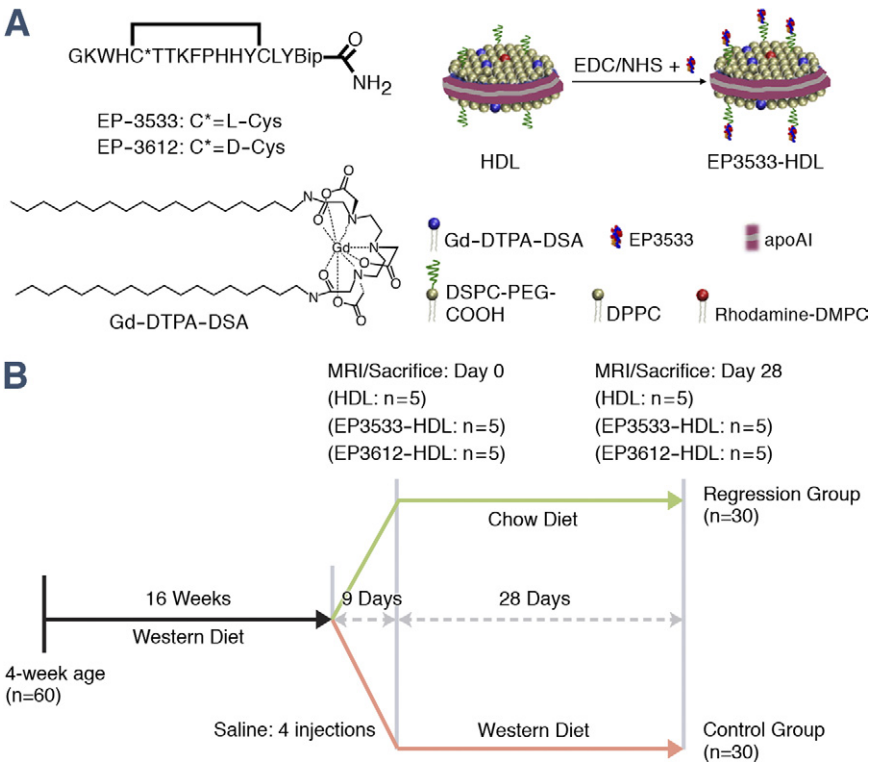

Figure 1. Chemical Structures and Experiment Design

Illustration of **(A)** method to functionalize high-density lipoprotein (HDL) nanoparticles with collagen-specific EP3553 peptides (named as EP3533-HDL) and **(B)** animal experiment design. apo A-I = apolipoprotein A-I; DPPC = 1,2-Dipalmitoyl-sn-glycero-3-phosphocholine; DSPC-PEG-COOH = 1,2-distearoyl-sn-glycero-3-phosphoethanolamine-*N*-[carboxy(polyethylene glycol)-2000] ammonium salt; EDC = 1-ethyl-3-[3-dimethylaminopropyl]carbodiimide hydrochloride; GD-DPTA-DSA = gadolinium diethylenetriaminepentaacetate-bis(stearylamide); MRI = magnetic resonance imaging; NHS = *N*-hydroxysuccinimide; pIpC = polyinsinic-polycytidylic ribonucleic acid; rhodamine-DMPC = 1,2-dimyristoyl-sn-glycero-3-phosphoethanolamine-*N*-(lissamine rhodamine B sulfonyl).

(22–26), but we included 1,2-distearoyl-sn-glycero-3-phosphoethanolamine-*N*-[carboxy(polyethylene glycol)-2000] ammonium salt (Avanti Polar Lipids, Inc.) to allow the peptides to attach.

PREPARATION OF EP3533-HDL AND EP3612-HDL NANOPARTICLES. The conjugation of EP-3533 peptides to HDL nanoparticles is schematically illustrated in Figure 1. First, the HDL nanoparticles were transferred into 4-(2-hydroxyethyl)-1-piperazineethanesulfonic acid buffer (pH = 5.0) and reacted with 1-ethyl-3-[3-dimethylaminopropyl]carbodiimide hydrochloride and *N*-hydroxysuccinimide. After incubation at room temperature for 2 h, the reaction solution was thoroughly washed. Then 1 mg/ml EP-3533 peptides in dimethyl sulfoxide was added into the solution with a 1:1.1 1,2-distearoyl-sn-glycero-3-phosphoethanolamine-*N*-[carboxy(polyethylene glycol)-2000] ammonium salt/EP-3533 molar ratio. This preparation was kept at room temperature for 4 h, stored at 4°C overnight, and then purified and buffer exchanged to phosphate-buffered saline (PBS). The final nanoparticles were named EP3533-HDL.

Nonspecific control nanoparticles (EP3612-HDL) were prepared by the same procedure using EP-3612 peptides.

IN VITRO BINDING ASSAY. Black 96-well plates were incubated with different proteins overnight at 4°C and then washed with PBS. After blocking with 2% bovine serum albumin (BSA) for 3 h at 37°C, they were washed again with PBS. Then nanoparticles were added to each well and incubated 3 h at 37°C. After cooling to room temperature, the total fluorescence I_0 of nanoparticles was recorded (excitation: 540 ± 25 nm; emission: 590 ± 35 nm). Then the nanoparticle solutions were aspirated. The plates were washed 3 times with PBS, after which the binding fluorescence I_{bind} was recorded. The average fluorescence reading of empty wells I_{empty} was subtracted from the raw fluorescence data. To correct the loss of

fluorescence labeling of 1,2-dimyristoyl-sn-glycero-3-phosphoethanolamine-*N*-(lissamine rhodamine B sulfonyl)from nanoparticles during peptide conjugation, the binding of nanoparticles was normalized as Normalized Binding = $(I_{bind} - I_{empty})/(I_0 - I_{empty})$*[Gd].

ANIMAL USE. The Institutional Animal Care and Use Committee of Mount Sinai School of Medicine approved the animal protocols and procedures. At 4 weeks of age, Reversa mice were weaned and then fed on Western diet containing a 0.15% cholesterol and 21% fat for 16 weeks. Mice were then divided into "regression" and control groups as shown in Figure 1. The regression group was fed on a chow diet and *Cre* was induced by intraperitoneal injection of polyinosinic-polycytidylic ribonucleic acid (250 μg every other day for a total of 4 injections). Day 0 was defined as the ninth day after first polyinosinic-polycytidylic ribonucleic acid injection. The mice were scanned by MR imaging at day 0 (n = 5) and day 28 (n = 5) and then sacrificed for histological staining. The control group was fed the Western diet for the duration of the experiment and injected with saline.

MR IMAGING. The animals underwent in vivo MR imaging of the abdominal aorta using a 9.4-T, 89-mm bore magnet system. High-resolution T_1-weighted images were generated using a black blood spin echo sequence (repetition time/echo time = 800 ms/8.6 ms, field of view = 3.0 × 3.0 cm, matrix size = 256 × 256, 22 contiguous 500 μm-thick axial slices, number of averages = 16, total scan time = 54 min). After pre-injection imaging, the animals were administered a nanoparticle contrast agent (50 μmol of Gd/kg) via the tail vein. Post-injection imaging with the same parameters was performed on each animal at 24 h after injection. The slices of the post-injection scan were matched to the pre-injection scan by using unique vertebral and paraspinous muscular anatomy as landmarks.

IMMUNOHISTOCHEMISTRY. Frozen abdominal aorta sections were stained using as primary antibodies either rat antimouse CD68 (Serotec, Raleigh, North Carolina) or rabbit antimouse collagen I (COL1A2:M-80, Santa Cruz Biotechnology Inc., Dallas, Texas). The secondary antibody was Alexa Fluor 647 conjugated goat antirat Ab or Alexa Fluor 647 conjugated goat antirabbit Ab (Serotec) corresponding to the primary antibody. Confocal imaging was performed using a

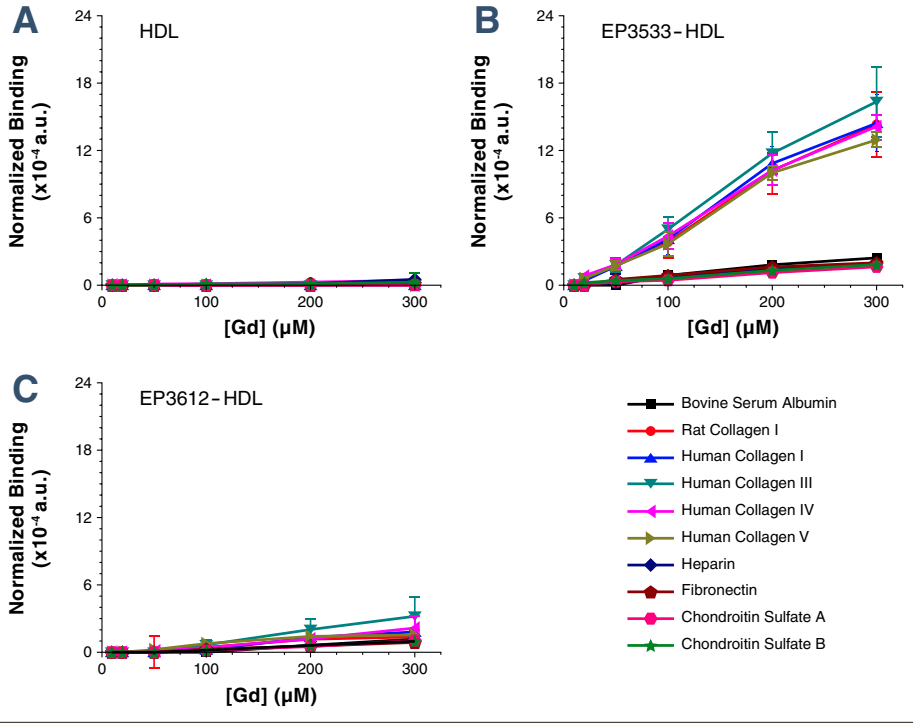

Figure 2. In Vitro Binding of Nanoparticles

Normalized in vitro binding of **(A)** high-density lipoprotein (HDL), **(B)** EP3533-HDL, and **(C)** EP3612-HDL nanoparticles to different proteins.

Leica SP5DM microscope (Buffalo Grove, Illinois).

Frozen sections were stained by Sirius red (Polysciences, Warrington, Pennsylvania) to detect interstitial collagen using birefringency illumination with polarized light.

For immunohistochemical CD68 staining, the frozen sections were stained using a rat antimouse CD68 primary antibody (Serotec). The sections were visualized using Vector Red solution for positive areas and counterstained blue with Vector Hematoxylin QS (Vector Laboratories, Inc., Burlingame, California).

IMAGE ANALYSIS. For in vivo MR images, the signal-to-noise ratio (SNR) of the region of interest (ROI) is defined by $SNR_{ROI} = I_{ROI}/I_{noise}$, where I_{ROI} is the intensity of either aortic vessel wall (SNR_w) or surrounding muscle (SNR_m); I_{noise} is the standard deviation outside the animal. The contrast-to-noise ratio (CNR) from the aortic wall to muscle is defined as $CNR_w = SNR_w - SNR_m$. The difference of CNR_w between pre- and post-injection is defined as $\Delta CNR_w = (CNR_w)_{post} - (CNR_w)_{pre}$. The normalized enhancement ratio (NER) of aortic wall to muscle is defined as $NER_w = [(SNR_w/SNR_m)_{post} - (SNR_w/SNR_m)_{pre}]/(SNR_w/SNR_m)_{pre} \times 100\%$. For ex vivo microscopy images, the percentages of positive area for macrophage and collagen contents were analyzed in ImageJ (W. S. Rasband, National Institutes of Health, Bethesda, Maryland) as described in the Online Appendix.

STATISTICS. The detailed statistical methods are described in the Online Appendix. A value of $p < 0.05$ was considered statistically significant.

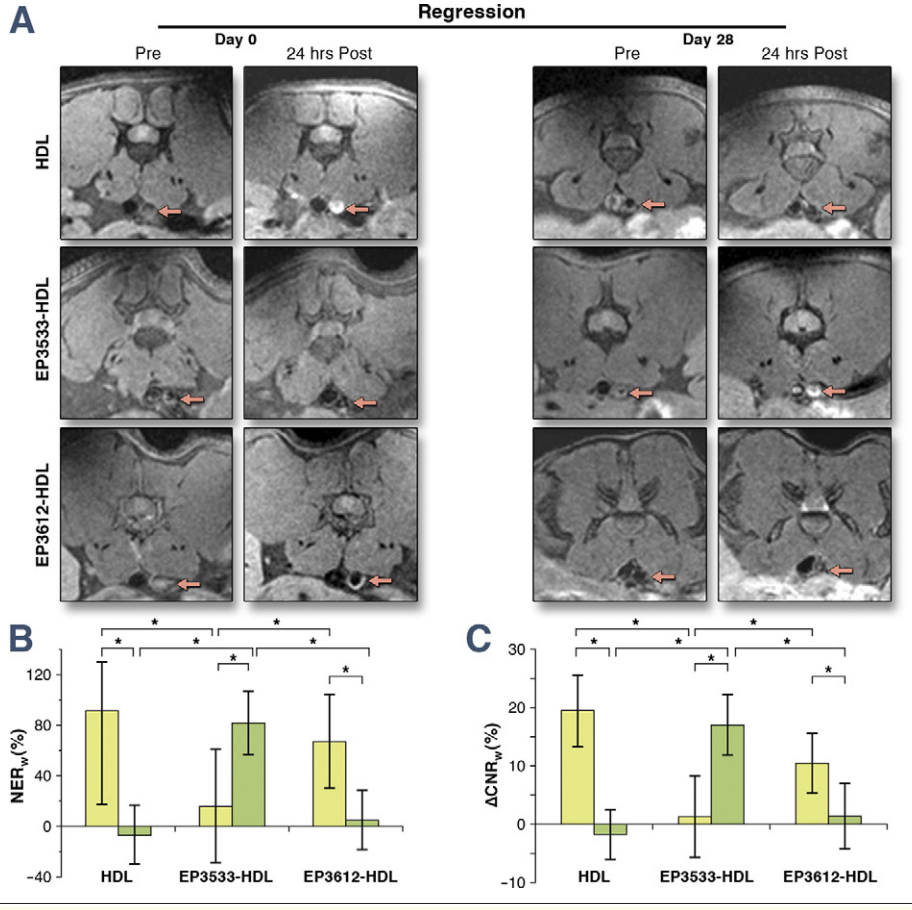

Figure 3. In Vivo MR Images of Regressed Plaques

(A) Typical MR images, **(B)** NER_w, and **(C)** ΔCNR_w of abdominal atherosclerotic plaques for pre- and 24 h post-injection of HDL, EP3533-HDL, and EP3612-HDL at day 0 **(yellow bars)** and day 28 **(green bars)** of Reversa mice in the regression group. The **arrows** point to the aortas. The error bars represent mean ± SD. The asterisks **(*)** indicate statistical significance at $p < 0.05$ ($n = 5$ mice × 5 slices/mice = 25). CNR = contrast-to-noise ratio; NER = normalized enhancement ratio; w = aortic vessel wall; other abbreviations as in Figure 1.

RESULTS

EP3533-HDL nanoparticles showed higher association with collagen in vitro than in control group. The conjugation of EP3533 or EP3612 peptides to HDL via 1,2-distearoyl-sn-glycero-3-phosphoethanolamine-*N*-[carboxy(polyethylene glycol)-2000] ammonium salt linkers did not significantly change the nanoparticle size (10 ± 2 nm) or longitudinal relaxivity (9 ± 1 s^{-1} $mmol/l^{-1}$). Figure 2A showed the unmodified HDL had negligible and lowest in vitro association with all the tested proteins among all 3 types of nanoparticles. EP3533-HDL (Fig. 2B), however, had significantly higher levels of binding to collagen in comparison with HDL and nonspecific EP3612-HDL and a low level of association to other extracellular matrix components, such as heparin, fibronectin, chondroitin sulfate A, and chondroitin sulfate B. The nonspecific EP3612-HDL (Fig. 2C) had much lower levels of association to all the tested collagen and other extracellular matrix components in comparison with EP3533-HDL, but slightly higher ones than unmodified HDL.

EP3533-HDL enhanced in vivo MR signal of aortic walls of regressing atherosclerotic plaques in Reversa mice. Representative in vivo MR images of atherosclerotic plaques of Reversa mice in the regression group are shown in Figure 3A. At day 0, the baseline of the regression, HDL caused enhancement of aortic vessel walls at 24 h after injection. However, EP3533-HDL did not cause significant enhancement. Nonspecific EP3612-HDL injection also induced signal enhancement of MR images of aortic vessel walls. The NER_w for HDL, EP3533-HDL, and EP3612-HDL contrast agents were 91 ± 39%, 16 ± 45%, and 67 ± 37%, respectively, at 24 h after injection (Fig. 3B). At day 28 of

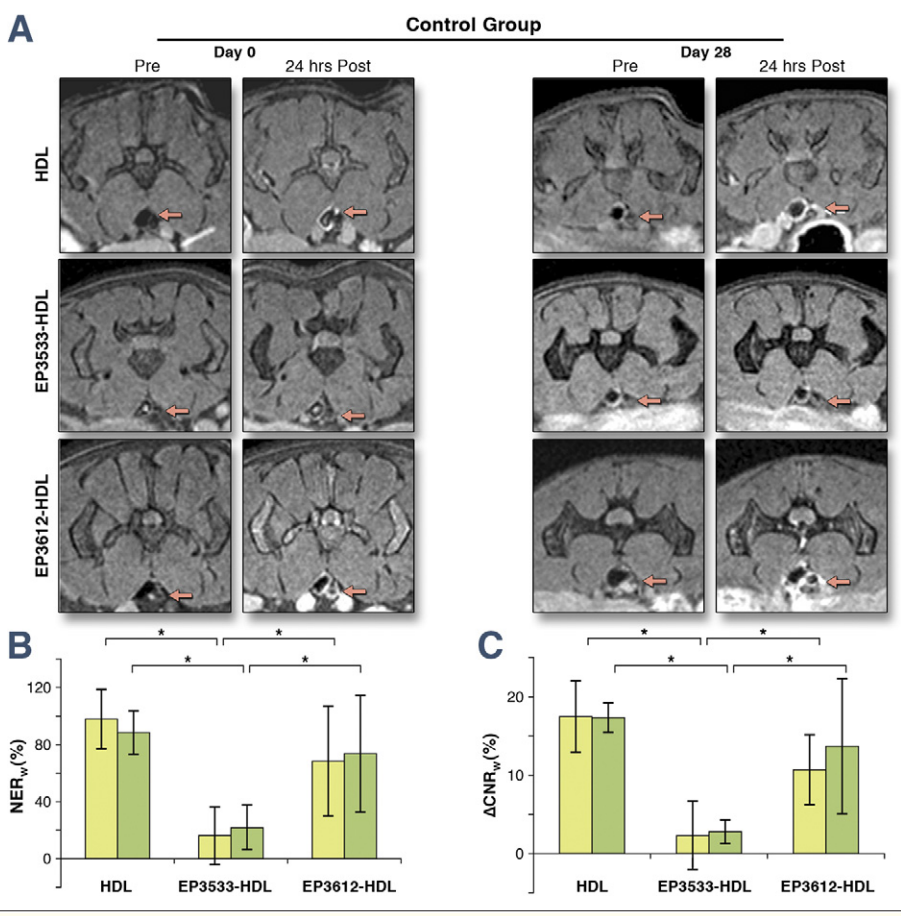

Figure 4. In Vivo MR Images of Control Plaques

(A) Typical MR images, **(B)** NER_w, and **(C)** ΔCNR_w of abdominal atherosclerotic plaques for pre- and 24 h post-injection of HDL, EP3533-HDL, and EP3612-HDL at days 0 and 28 of Reversa mice in the control group (n = 5 mice × 5 slices/mice = 25). Abbreviations as in Figures 1 and 3.

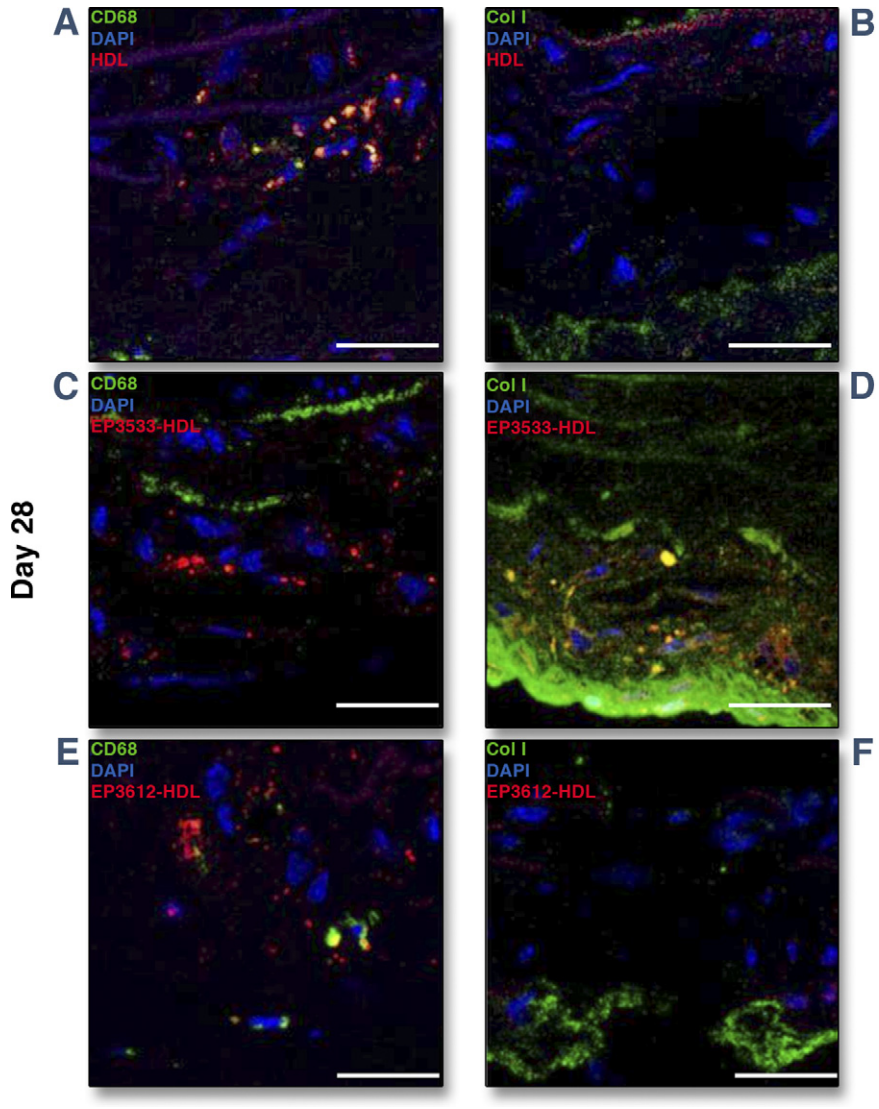

Figure 5. Colocalization of Nanoparticles

Confocal microscopy of plaques at day 28 from aortic vessel walls of Reversa mice in the regression group with **(A, C, E)** CD68 **(green)** or **(B, D, F)** collagen type I (Col I) **(green)** staining. The nuclei were stained with 4,6-diamino-2-phenylindole (DAPI) **(blue)** and nanoparticles were labeled with 1,2-dimyristoyl-sn-glycero-3-phosphoethanolamine-*N*-(lissamine rhodamine B sulfonyl) (rhodamine-PE) **(red).** The colocalization of **green** and **red** signals appeared as **yellow/orange colors.** Scale bar: 25 μm. HDL = high-density lipoprotein.

regression, the signal enhancements or NER_w induced by the injection of HDL and EP3612-HDL were substantially reduced to $-7 \pm 23\%$ and $4 \pm 24\%$, respectively, at 24 h after injection. In comparison, the enhancement caused by EP3533-HDL increased significantly to $82 \pm 25\%$ at 24 h after injection (Fig. 3B). The corresponding ΔCNR_w values are shown in Figure 3C, which showed the same trends as NER_w. In the control group (i.e., continuing hyperlipidemia), the NER_w and the ΔCNR_w of all 3 nanoparticle contrast agents remained similar at day 28, with values in comparison with those at day 0 baseline (Fig. 4).

EP3533-HDL nanoparticles showed colocalization with collagen type I in aortic vessel walls of Reversa mice at day 28 in the regression group. After in vivo MR imaging, the colocalization of nanoparticles was analyzed on aortic sections at 24 h after injection of contrast agents. The HDL nanoparticles were found to localize mainly with macrophages at day 28 (Fig. 5A), in agreement with previous results (22–25), but not with collagen type I (Fig. 5B). At

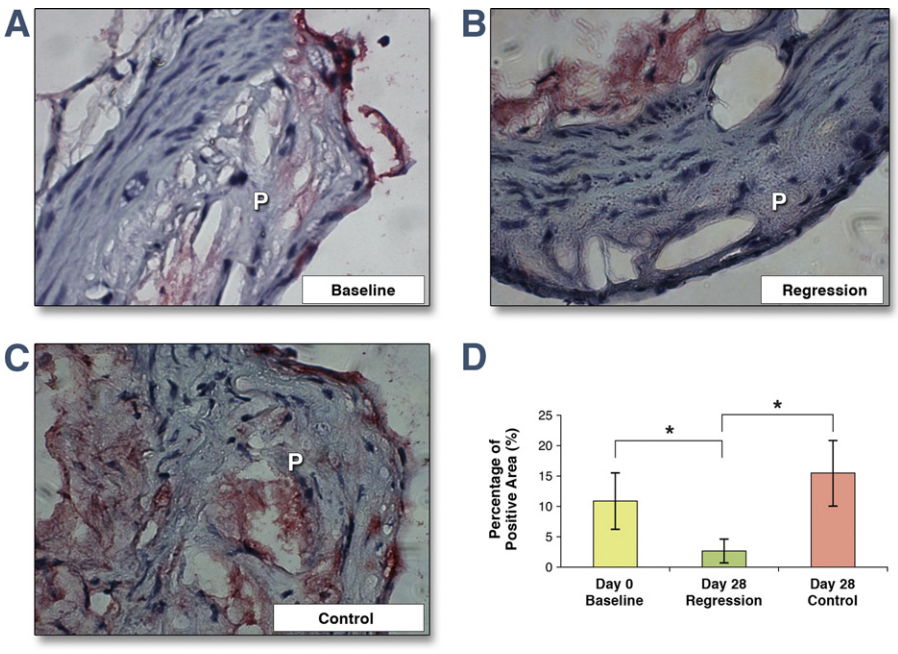

Figure 6. Intraplaque Macrophage Contents

Immunohistochemical staining of CD68+ macrophages **(red)** in the atherosclerotic plaques of aorta at **(A)** day 0 and day 28 in **(B)** regression and **(C)** control groups. Nuclei in **blue. (D)** The percentage of CD68+ area in the plaques. The images were obtained at 40× (n = 5). P = plaque position.

day 28, EP3533-HDL was found to localize with collagen type I (Fig. 5D) with negligible association with CD68 signal under confocal imaging (Fig. 5C). Most of the nonspecific EP3612-HDL was not found to localize with CD68+ macrophages or collagen type I at day 28, though some of these nanoparticles were seen at the same positions of CD68 signals in confocal images (Figs. 5E and 5F). Confocal microscopy of all 3 types of nanoparticles with CD68 macrophages and collagen type I staining at day 0 is available in the Online Appendix.

The content of CD68+ cells decreased at day 28 in aortic plaques of Reversa mice in the regression group. The area percentage of CD68+ macrophages/foam cells (red) was 10.9 ± 4.6% in the plaques at day 0 (Figs. 6A and 6D). At day 28 of regression, the CD68+ cells decreased significantly to 2.6 ± 2.0% (Figs. 6B and 6D). However, the content of CD68+ area increased to 15.5 ± 5.4% at day 28 in the control group (Figs. 6C and 6D).

The collagen content increased at day 28 in aortic plaques of Reversa mice in the regression group. As shown in Figure 7A, the plaques at aortic vessel walls at day 0 showed little collagen (from analysis of polarized light images) corresponding to a collagen positive area of 2.9 ± 2.1% (Fig. 7D). At day 28, the collagen content increased significantly to 22.1 ± 11.6% in the regression group (Figs. 7B and 7D). However, the collagen content maintained a similar level (2.0 ± 0.7% of plaques) at day 28 in the control group (Figs. 7C and 7D). The red stained areas were observed under bright field but not always as fibrils under polarized light in Figure 7C. This suggests that not all the collagen was organized into fibrils but rather some was degraded by matrix metalloproteinases expressed by macrophages or foam cells.

The percentage of macrophage or collagen positive area was pooled together from both the regression and control groups to establish the correlations with in vivo MR enhancement (NER_w in the aortic walls). The correlation coefficients were 0.85 (R^2 = 0.71) for CD68+ macrophages with in vivo NER_w from HDL injection (Fig. 8A) and 0.77 (R^2 = 0.60) for collagen with in vivo NER_w from EP3533-HDL injection (Fig. 8B).

DISCUSSION

In the present study, we demonstrated that HDL-based nanoparticles can be used as MR contrast agents for noninvasive in vivo imaging of atherosclerotic plaque regression by targeting collagen after conjugation with collagen-specific EP3533

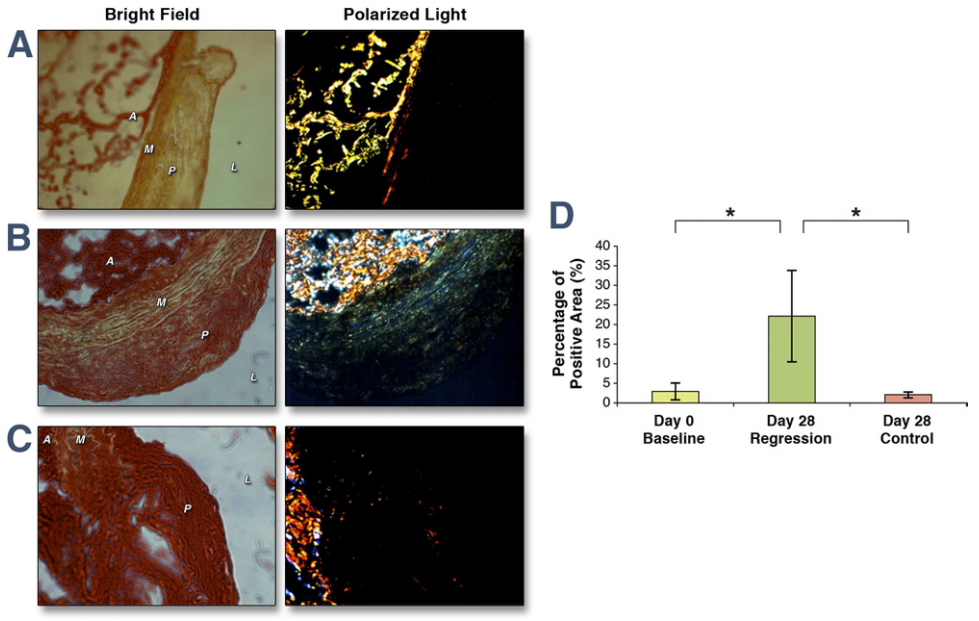

Figure 7. Intraplaque Collagen Contents

Sirius red staining of atherosclerotic plaques in aortic vessel walls at **(A)** day 0 and day 28 in **(B)** regression and **(C)** control groups. The bright field images indicate the position of plaques. The collagen containing area is bright under polarized light. **(D)** The percentage of collagen-positive area in the plaques (n = 5). *A* = adventitia position; *L* = lumen position; *M* = media position; *P* = plaque position.

peptides. The interaction between HDL and collagen is improved by the EP3533 peptides (Fig. 2), which have been developed to specifically target collagen (27). It is likely that EP3533-HDL may bind to collagen in the media and adventitia as well as in the plaque in vivo. Unfortunately, the resolution required to distinguish among the media, adventitia, and plaque in mice arteries is not currently possible, although the contrast changes we observed are most likely due to changes in collagen in the plaque and not other parts of the arterial wall.

Macrophages and collagen play important roles in the vulnerability of atherosclerotic plaques. Macrophage content has been used to evaluate atherosclerotic plaque burden in animal models and in humans (26,28–33). Feig et al. (17) reported a detailed study of biological characteristics of Reversa mice, which was confirmed again in this study (Figs. 6 and 7). In advanced plaques, collagen fibrils are degraded by matrix metalloproteinases, resulting in many small fragments, which were not observed under polarized light microscopy or seen to associate with EP3533-HDL. The MR imaging and histology results together also likely imply that EP3533-HDL is targeting collagen fibrils as opposed to degraded collagen. It should be noted that rather than providing an absolute amount of collagen, EP3533-HDL indicates a relative collagen level in plaques by MR imaging.

The different trends of macrophage and collagen contents during plaque regression were found to be correlated with the in vivo MR signals of aortic vessel walls using HDL and EP3533-HDL as contrast agents (Fig. 8). The correlations indicated the MR signals from aortic vessel walls are most likely reflecting the macrophage and collagen contents. Therefore, collagen-specific EP3533-HDL nanoparticles can be used to visualize the collagen content noninvasively in vivo and thus to monitor the characteristics that are taken to indicate the stabilization of human atherosclerotic plaques after therapeutic intervention.

HDL nanoparticles were found to be mainly colocalized with CD68+ macrophages at both baseline (day 0) (Online Fig. 1) and day 28 of regression (Fig. 5A). These results are consistent with our previous findings in several other mouse models (22–25). We also observed that not all HDL nanoparticles are associated with macrophages, which may be due to the retention of HDL by proteoglycans, especially biglycan and perlecan (34–35) from the association of apolipoprotein A-I in the lipid pools (36–38) and around necrotic cores (39) in atherosclerotic plaques. Interestingly, at

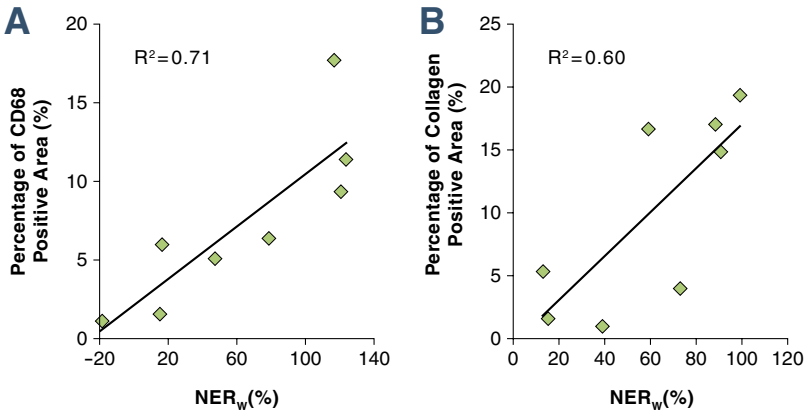

Figure 8. Correlations of MR Images With Macrophages and Collagens

Correlations of **(A)** CD68+ and **(B)** collagen-positive areas with NER_w obtained after HDL and EP3533-HDL injections, respectively. Abbreviations as in Figures 1 and 3.

baseline (day 0), EP3533-HDL was also found to be associated with CD68+ macrophages and had a low association with collagen type I (Online Fig. 1). This could be due to several reasons. First, activated high levels of macrophages in plaques at day 0 could take up EP3533-HDL through nonspecific endocytosis or phagocytosis. Second, conjugation of EP3533 cannot fully block HDL function, leading to off-target macrophage association. Third, the very low content of collagen results in little interaction with EP3533-HDL. However, at day 28 under regression conditions, EP3533-HDL was found to be associated with collagen type I–rich areas inside plaque due to strong binding to collagen (Fig. 2A) and the readily accessible collagen contents inside plaque (Figs. 7B and 7D), but it was not found to be associated with CD68+ macrophages due to low macrophage content (Figs. 6B and 6D) and the low possibility of access to nanoparticles. Little accumulation of EP3533-HDL was observed in the adventitia because the intravenously injected nanoparticles remained primarily inside lumen and minimally reached adventitia, which typically has little vasa vasorum compared with human plaques.

CONCLUSIONS

We demonstrate that HDL-based nanoparticles are a versatile platform to noninvasively image atherosclerosis in vivo by MR to visualize not only macrophages, but also collagen after conjugation to HDL of collagen-specific peptides, which provides a rerouting strategy. MR signal enhancements of atherosclerotic plaques in aortic vessel walls after HDL and EP3533-HDL injections in Reversa mice were correlated with macrophage and collagen contents, respectively. By combination of imaging macrophage and collagen contents, the stabilization process of atherosclerotic plaques can be monitored and evaluated in vivo under regression conditions.

Acknowledgments

Confocal microscopy was performed at the Microscopy Shared Resource Facility which is supported by the following grants: NIH-NCI 5R24 CA095823-04, NSF DBI-9724504, and NIH 1 S10 RR0 9145-01.

Reprint requests and correspondence: Dr. Zahi A. Fayad, Icahn School of Medicine at Mount Sinai, Translational and Molecular Imaging Institute, One Gustave L. Levy Place, New York, New York 10029. *E-mail: zahi.fayad@mssm.edu.* OR Dr. Edward A. Fisher, New York University School of Medicine, Smilow 8, 522 First Avenue, New York, New York 10016. *E-mail: edward.fisher@nyumc.org.*

REFERENCES

1. Fuster V, Moreno PR, Fayad ZA, Corti RC, Badimon JJ. Atherothrombosis and high-risk plaque: part I: evolving concepts. J Am Coll Cardiol 2005;46:937–54.
2. Fuster V, Fayad ZA, Moreno PR, Poon M, Corti R, Badimon JJ. Atherothrombosis and high-risk plaque: part II: approaches by noninvasive computed tomographic/magnetic resonance imaging. J Am Coll Cardiol 2005;46:1209–18.
3. Stary HC. Natural history and histological classification of atherosclerotic lesions: an update. Arterioscler Thromb Vasc Biol 2000;20:1177–8.
4. Rosamond W, Flegal K, Friday G, et al. Heart disease and stroke statistics—2007 update: a report from the American Heart Association Statistics Committee and Stroke Statistics Subcommittee. Circulation 2007;115:e69–171.
5. Yuan C, Mitsumori LM, Ferguson MS, et al. In vivo accuracy of multispectral magnetic resonance imaging for identifying lipid-rich necrotic cores and intraplaque hemorrhage in advanced human carotid plaques. Circulation 2001;104:2051–6.
6. Albuquerque LC, Narvaes LB, Maciel AA, et al. Intraplaque hemorrhage assessed by high-resolution magnetic resonance imaging and C-reactive protein in carotid atherosclerosis. J Vasc Surg 2007;46:1130–7.
7. Kang HW, Torres D, Wald L, Weissleder R, Bogdanov AA. Targeted imaging of human endothelial-specific marker in a model of adoptive cell transfer. Lab Invest 2006;86:599–609.
8. Winter PM, Neubauer AM, Caruthers SD, et al. Endothelial alpha (v)beta3 integrin-targeted fumagillin nanoparticles inhibit angiogenesis in atherosclerosis. Arterioscler Thromb Vasc Biol 2006;26:2103–9.
9. Winter PM, Morawski AM, Caruthers SD, et al. Molecular imaging of angiogenesis in early-stage atherosclerosis with alpha(v)beta3 -integrin-targeted nanoparticles. Circulation 2003;108:2270–4.
10. Papaioannou TG, Vavuranakis M, Androulakis A, et al. In-vivo imaging of carotid plaque neoangiogenesis with contrast-enhanced harmonic ultrasound. Int J Cardiol 2009;134:e110–2.
11. Virmani R, Kolodgie FD, Burke AP, et al. Atherosclerotic plaque progression and vulnerability to rupture: angiogenesis as a source of intraplaque hemorrhage. Arterioscler Thromb Vasc Biol 2005;25:2054–61.
12. Crisby M, Nordin-Fredriksson G, Shah PK, Yano J, Zhu J, Nilsson J. Pravastatin treatment increases collagen content and decreases lipid content, inflammation, metalloproteinases, and cell death in human carotid plaques: implications for plaque stabilization. Circulation 2001;103:926–33.
13. Aikawa M, Rabkin E, Okada Y, et al. Lipid lowering by diet reduces matrix metalloproteinase activity and increases collagen content of rabbit atheroma: a potential mechanism of lesion stabilization. Circulation 1998;97:2433–44.
14. Llodrá J, Angeli V, Liu J, Trogan E, Fisher EA, Randolph GJ. Emigration of monocyte-derived cells from atherosclerotic lesions characterizes regressive, but not progressive, plaques. Proc Natl Acad Sci U S A 2004;101:11779–84.
15. Trogan E, Feig JE, Dogan S, et al. Gene expression changes in foam cells and the role of chemokine receptor CCR7 during atherosclerosis regression in ApoE-deficient mice. Proc Natl Acad Sci U S A 2006;103:3781–6.
16. Lieu HD, Withycombe SK, Walker Q, et al. Eliminating atherogenesis in mice by switching off hepatic lipoprotein secretion. Circulation 2003;107:1315–21.
17. Feig JE, Parathath S, Rong JX, et al. Reversal of hyperlipidemia with a genetic switch favorably affects the content and inflammatory state of macrophages in atherosclerotic plaques. Circulation 2011;123:989–98.
18. Saam T, Hatsukami TS, Takaya N, et al. The vulnerable, or high-risk, atherosclerotic plaque: noninvasive MR imaging for characterization and assessment. Radiology 2007;244:64–77.
19. Mulder WJ, Strijkers GJ, Briley-Saboe KC, et al. Molecular imaging of macrophages in atherosclerotic plaques using bimodal PEG-micelles. Magn Reson Med 2007;58:1164–70.
20. Choudhury RP, Fuster V, Fayad ZA. Molecular, cellular and functional imaging of atherothrombosis. Nat Rev Drug Discov 2004;3:913–25.
21. Sanz J, Fayad ZA. Imaging of atherosclerotic cardiovascular disease. Nature 2008;451:953–7.
22. Frias JC, Ma YQ, Williams KJ, Fayad ZA, Fisher EA. Properties of a versatile nanoparticle platform contrast agent to image and characterize atherosclerotic plaques by magnetic resonance imaging. Nano Lett 2006;6:2220–4.
23. Frias JC, Williams KJ, Fisher EA, Fayad ZA. Recombinant HDL-like nanoparticles: a specific contrast agent for MRI of atherosclerotic plaques. J Am Chem Soc 2004;126:16316–7.
24. Chen W, Vucic E, Leupold E, et al. Incorporation of an apoE-derived lipopeptide in high-density lipoprotein MRI contrast agents for enhanced imaging of macrophages in atherosclerosis. Contrast Media Mol Imaging 2008;3:233–42.
25. Cormode DP, Skajaa T, van Schooneveld MM, et al. Nanocrystal core high-density lipoproteins: a multimodality contrast agent platform. Nano Lett 2008;8:3715–23.
26. Cormode DP, Briley-Saebo KC, Mulder WJ, et al. An ApoA-I mimic peptide high-density-lipoprotein-based MRI contrast agent for atherosclerotic plaque composition detection. Small 2008;4:1437–44.
27. Caravan P, Das B, Dumas S, et al. Collagen-targeted MRI contrast agent for molecular imaging of fibrosis. Angew Chem Int Ed Engl 2007;46:8171–3.
28. Stary HC, Chandler AB, Dinsmore RE, et al. A definition of advanced types of atherosclerotic lesions and a histological classification of atherosclerosis: a report from the Committee on Vascular Lesions of the Council on Arteriosclerosis, American Heart Association. Circulation 1995;92:1355–74.
29. Ruehm SG, Corot C, Vogt P, Kolb S, Debatin JF. Magnetic resonance imaging of atherosclerotic plaque with ultrasmall superparamagnetic particles of iron oxide in hyperlipidemic rabbits. Circulation 2001;103:415–22.
30. Gronholdt ML, Nordestgaard BG, Bentzon J, et al. Macrophages are associated with lipid-rich carotid artery plaques, echolucency on B-mode imaging, and elevated plasma lipid levels. J Vasc Surg 2002;35:137–45.
31. Choudhury RP, Lee JM, Greaves DR. Mechanisms of disease: macrophage-derived foam cells emerging as therapeutic targets in atherosclerosis. Nat Clin Pract Cardiovasc Med 2005;2:309–15.
32. Davies JR, Rudd JF, Fryer TD, Weissberg PL. Targeting the vulnerable plaque: the evolving role of nuclear imaging. J Nucl Cardiol 2005;12:234–46.
33. Trogan E, Fayad ZA, Itskovich VV, et al. Serial studies of mouse atherosclerosis by in vivo magnetic resonance imaging detect lesion regression after correction of dyslipidemia. Arterioscler Thromb Vasc Biol 2004;24:1714–9.
34. O'Brien KD, McDonald TO, Kunjathoor V, et al. Serum amyloid A and lipoprotein retention in murine models of atherosclerosis. Arterioscler Thromb Vasc Biol 2005;25:785–90.

35. Kunjathoor VV, Chiu DS, O'Brien KD, LeBoeuf RC. Accumulation of biglycan and perlecan, but not versican, in lesions of murine models of atherosclerosis. Arterioscler Thromb Vasc Biol 2002;22:462–8.
36. Hoff HF, Heideman CL, Jackson RL, Bayardo RJ, Kim HS, Gotto AM Jr. Localization patterns of plasma apolipoproteins in human atherosclerotic lesions. Circ Res 1975;37:72–9.
37. Hoff HF. Apolipoprotein localization in human cranial arteries, coronary arteries, and the aorta. Stroke 1976;7:390–3.
38. Carter RS, Siegel RJ, Chai AU, Fishbein MC. Immunohistochemical localization of apolipoproteins A-I and B in human carotid arteries. J Pathol 1987;153:31–6.
39. Bedossa P, Poynard T, Abella A, Paraf F, Lemaigre G, Martin E. Localization of apolipoprotein A-I and apolipoprotein A-II in human atherosclerotic arteries. Arch Pathol Lab Med 1989;113:777–80.

Key Words: collagen ■ high-density lipoprotein ■ macrophage ■ magnetic resonance imaging ■ nanoparticles.

▶APPENDIX

For detailed experimental and statistical methods, confocal images for mice at Day 0 in regression group, and split channel images for Figure 5D, please see the online version of this paper.